



**HAL**  
open science

## Effect of innovative microwave assisted freezing (MAF) on the quality attributes of apples and potatoes

Piyush Kumar Jha, S. Chevallier, Epameinondas Xanthakis, Vanessa Jury,  
Alain E Le-Bail

### ► To cite this version:

Piyush Kumar Jha, S. Chevallier, Epameinondas Xanthakis, Vanessa Jury, Alain E Le-Bail. Effect of innovative microwave assisted freezing (MAF) on the quality attributes of apples and potatoes. Food Chemistry, 2020, 309, pp.1-12. 10.1016/j.foodchem.2019.125594 . hal-02465818

**HAL Id: hal-02465818**

**<https://hal.science/hal-02465818>**

Submitted on 20 Jul 2022

**HAL** is a multi-disciplinary open access archive for the deposit and dissemination of scientific research documents, whether they are published or not. The documents may come from teaching and research institutions in France or abroad, or from public or private research centers.

L'archive ouverte pluridisciplinaire **HAL**, est destinée au dépôt et à la diffusion de documents scientifiques de niveau recherche, publiés ou non, émanant des établissements d'enseignement et de recherche français ou étrangers, des laboratoires publics ou privés.



Distributed under a Creative Commons Attribution - NonCommercial 4.0 International License

1  
2  
3  
4  
5  
6  
7  
8  
9  
10  
11  
12  
13  
14  
15  
16  
17  
18  
19  
20  
21  
22  
23  
24  
25  
26  
27  
28  
29  
30  
31

**Effect of innovative microwave assisted freezing (MAF) on the quality attributes of apples and potatoes**

**Piyush Kumar Jha<sup>a, b</sup>, Sylvie Chevallier<sup>a, b</sup>, Epameinondas Xanthakis<sup>c</sup>, Vanessa Jury<sup>a, b</sup>, Alain Le-Bail<sup>a, b</sup>**

<sup>a</sup> ONIRIS, CS 82225, 44322 Nantes cedex 3, France  
<sup>b</sup> UMR GEPEA CNRS 6144 - ONIRIS, 44322 Nantes cedex 3, France  
<sup>c</sup> RISE-Agrifood & Bioscience, Gothenburg, Sweden

**Abstract**

This study considered the effect of low energy microwave assisted freezing (MAF) on freezing time and quality attributes (microstructure, texture, drip loss and colour) of apple and potato. MAF of apples and potatoes was performed by applying constant microwave (MW) power (167W/kg) and pulsed MW power (500 and 667W/kg with 10s pulse width and 20s pulse interval resulting in an average power of 167 and 222W/kg) during the freezing process. The temperature profile was monitored during the freezing process, and the microstructure was examined using X-ray micro-tomography and cryo-SEM. Other quality parameters such as texture, drip loss and colour were evaluated with thawed samples. It appeared that the freezing time was not affected by the MAF process. It is the first time that a MAF process is used for freezing plant-based products and showed that the application of microwaves during freezing process caused less freeze damage than the control condition.

**KEYWORDS (8)**  
freezing; microstructure; quality; microwave; SEM; drip loss; potato; apple

## 32 **1. Introduction**

33 Freeze damage in the cellular matrices is a major challenge for the food industries. Several  
34 strategies from conventional to innovative methods have been used to minimize such  
35 drawback. Conventional methods typically include the use of (i) improved freezing conditions  
36 (i.e. use of higher freezing rate) and (ii) pre-freezing treatments (infusion of different  
37 substances such as  $\text{CaCl}_2$ , sucrose, pectin, cryoprotectants, minerals, etc. in the tissue system).  
38 In addition, there is a third track (iii) which focuses on the optimization of the thawing rate.  
39 With respect to the freezing of tissue systems, higher freezing rates are preferred over slow  
40 freezing rates, because numerous fine ice crystals are being produced in both intracellular and  
41 extracellular domains, and lead to less dislocation of water from the inner part of the cells to  
42 the extracellular domains. The damage of the tissue system is reduced due to less dehydration  
43 and shrinkage of the cell. Besides, fast freezing rates also reduce the denaturation of the  
44 proteins and other organized biopolymers that may occur due to the cryo-concentration effect.  
45 However, rapid freezing processes require high energy demands due to the need for very high  
46 heat transfer coefficient. Moreover, the use of very fast freezing rates may also develop cracks  
47 in the samples and thus degrade the quality of the final product (Shi, Datta, & Mukherjee,  
48 1999, 1998; Shi, Datta, & Throop, 1998).

49 In recent times, several novel freezing methods have been developed aiming to minimize  
50 freeze damage and to improve the quality of a frozen product. Those methods include freezing  
51 assisted by high-pressure shift (Koch, Seyderhelm, Wille, Kalichevsky, & Knorr, 1996);  
52 ultrasound waves (Sun & Li, 2003); electric fields (Xanthakis, Havet, Chevallier, Abadie, &  
53 Le-Bail, 2013); magnetic fields (Jha et al., 2017); and vacuum impregnation (Xie & Zhao  
54 (2003). Experimental studies have shown that it is possible to obtain smaller ice crystals after  
55 freezing assisted by electromagnetic waves. Hanyu, Ichikawa, & Matsumoto (1992) reported  
56 that MW irradiation (for 50 ms) followed by freezing produced smaller ice crystals in the  
57 frozen samples (squid retina, rat liver and heart muscle) with a good repeatability. Moreover,  
58 the zone of good freezing extended to a greater depth into the MW irradiated samples than the  
59 control. The zone of better freezing can be referred as the area where there is no sign of  
60 detectable ice-crystal damage. According to their study, MW irradiated sample had a larger  
61 ice-free (vitrified) region compared to the untreated samples. Jackson, Ungan, Critser, & Gao  
62 (1997) reported that the continuous application of MW (2.45 GHz and 1000 W) during  
63 vitrification of ethylene glycol solution (cryo-protectant) caused a significant reduction of ice  
64 formation. Anese et al. (2012) carried out another study on the application of electromagnetic  
65 radiation in the range of radio frequency (RF) waves during freezing of meat. Although no

66 data were presented on ice crystal size, the histological micrographs seemed to indicate that  
67 the ice crystal size decreased under RF assisted freezing conditions. Xanthakis et al. (2014)  
68 found smaller ice crystals and a decrease in the degree of supercooling under pulsed MW  
69 (2.45 GHz) assisted freezing. Moreover, they reported that freezing rate decreased when the  
70 power level of MW was increasing due to the heat generated by MWs. Their study provided  
71 quantitative data regarding the ice crystal size and the impact of MW radiation during  
72 freezing of meat. The improved microstructure highlighted the need for further investigation  
73 and the potential of this technology to be applied for the production of frozen food with  
74 improved quality. Most recently, Hafezparast-Moadab et al. (2018) performed pulsed RF  
75 (27.12 MHz) assisted air blast freezing of fish. The results revealed that the RF assisted frozen  
76 fish had finer ice crystals (up to 75% smaller by surface), lesser damage to the structure,  
77 lower drip loss, and superior texture (close to fresh sample) than sample frozen in the absence  
78 of RF.

79

80 To the best of our knowledge, MAF process has never been used for freezing plant based  
81 products before. The objective of this work was to expand the application of MAF to food  
82 commodities with more sensitive structures than meat such as fruits and vegetables. In order  
83 to explain the mechanism of action of MAF more conditions were investigated in depth by  
84 means of a more advanced MAF equipment, and more quality attributes were evaluated. This  
85 paper presents the results regarding freezing of fruits and vegetables under low power MW  
86 emission (2.45 GHz), the impact of MAF on the microstructure of the food matrices and their  
87 freeze damage compared to conventional freezing.

88

## 89 **2. Materials and Methods**

### 90 **2.1. Sample Preparations**

91 The apples (Royal Gala) were purchased from the local supermarket (E. Leclerc, Nantes,  
92 France) and stored at 2 °C until use (maximum 4 weeks). Cylindrical pieces of apple  
93 ( $0.47 \pm 0.03$  g) with a diameter ( $\emptyset$ ) of 8 mm and height (H) of 10 mm were cut using a sharp  
94 cylindrical punch in tangential orientation from the middle parenchyma of the fruit. At least 7  
95 cylinders were cut from each fruit in order to have a large number of samples aiming to  
96 reduce the variability caused by the inhomogeneity of fruit's structure. The samples were then  
97 placed in zip-lock bags and stored at  $4 \pm 1$  °C in order to avoid any moisture loss and to

98 achieve a uniform temperature prior to the freezing tests. The moisture content and freezable  
99 water amount apples used for this study were  $87.32 \pm 0.48\%$  (wet basis) and  $75.92 \pm 0.67\%$ .

100

101 A batch of potatoes (*Solanum tuberosum* L. cv. Innovator) which was used for the  
102 experiments of the entire study was provided by *McCain Foods*. Potato samples with  
103 dimensions ( $1.3 \times 1.3 \times 1 \text{ cm}^3$  – length  $\times$  height  $\times$  width) and weight ( $1.95 \pm 0.5 \text{ g}$ ) were cut  
104 and blanched prior to the freezing tests. The blanching of potato was performed by immersing  
105 around 500 g of samples in hot water ( $85 \pm 1 \text{ }^\circ\text{C}$ ) for 1 min 50 s. This blanching time fulfilled  
106 the criteria of adequate blanching for the specific cultivar, which requires the sample core  
107 temperature to be at  $75 \text{ }^\circ\text{C}$  for at least 1 min (*McCain Foods*). After blanching, the samples  
108 were cooled down to the room temperature by dipping in cold water at ambient temperature  
109 ( $20 \pm 1 \text{ }^\circ\text{C}$ ) for 9 min. The surface moisture of the samples was removed gently with  
110 absorbent paper. Finally, the samples were placed in a zip-lock bag and kept at  $4 \pm 1 \text{ }^\circ\text{C}$  to  
111 achieve a uniform temperature prior to the freezing tests. The average moisture content and  
112 freezable water content of potato were  $75.70 \pm 1.40\%$  and  $67.5 \pm 2.1\%$ .

113

## 114 **2.2. Microwave assisted freezer prototypes and different MAF freezing strategies**

115 Two experimental systems have been used in terms of refrigeration means. The MW cavity  
116 which was installed in a blast freezer (RS 10/RL, ACFRI, France) was used for MAF of  
117 apples (see Supplementary Data for a schematic representation of the equipment). The air  
118 inlet was the side entry and the outlet was the passage connected at the back wall of the  
119 cavity. In this experimental unit the airflow rate was fixed at 1.1 m/s.

120

121 In order to incorporate and investigate the impact of one extra parameter (higher heat transfer  
122 coefficient) in the latter experiments of potatoes, the experimental equipment was modified.  
123 In this experimental set-up the, MW cavity was installed in a large freezing cabinet (ca  $1 \text{ m}^3$ -  
124 MATAL, France). An air blower was connected to the air passage located at the back wall of  
125 the cavity offering the ability to adjust the airflow rate for this configuration in the range of 1  
126 to 3 m/s (a schematic representation of the equipment is provided in the Supplementary Data).  
127 The difference between air entry on side passage or back wall passage did not impact the  
128 freezing conditions since the crossed directions of the lateral and back wall passages resulted  
129 in a turbulent air flow within the cavity.

130

131 For both systems, the same domestic MW cavity was connected to a solid state MW emitter.  
132 The MWs of 2.45 GHz required for the freezing tests were generated using a solid-state  
133 generator with adjustable power up to 200 W (Sairem, Lyon, France). A pulse generator  
134 (fabricated in our lab) connected to the MW producing source helped to achieve selected MW  
135 emission with different length of pulses.

136 Prior to each freezing test, the freezing chamber was precooled at  $-30\text{ }^{\circ}\text{C}$  with 1.1 m/s (for  
137 apple) and 2.30-2.50 m/s (for potato) cold air flow. MAF of apples and potatoes was  
138 performed by placing the samples (30 g) in the freezing chamber and simultaneously applying  
139 MWs of various power levels. Four freezing conditions were studied, comprising one  
140 condition without MW exposure (control) and three under MW exposure. The three MW  
141 conditions included one microwave freezing condition under constant radiation (CMAF: 5 W  
142 or 167 W/kg applied continuously) and two microwave freezing conditions under pulsed  
143 radiation (P1MAF: 15 W or 500 W/kg with 10 s pulse width and 20 s pulse interval (average  
144 power = 167 W/kg) and P2MAF: 20 W or 667 W/kg with 10 s pulse width and 20 s pulse  
145 interval (average power = 222 W/kg)).

146 The time-temperature profile during the freezing tests was studied by inserting an optical fibre  
147 at the geometric centre of the product. The optical fibre was calibrated against a reference  
148 platinum probe (Comptoir Lyon Allemand – Lyon-France). During measurements  
149 temperature changes of the sample were recorded every 5 s by a data logger with accuracy of  
150  $\pm 0.1\text{ }^{\circ}\text{C}$ . The freezing tests were terminated once the geometric centre of the product reached  
151  $-18\text{ }^{\circ}\text{C}$ .

152 In this study, characteristic freezing time and overall freezing time were determined for each  
153 freezing condition. The characteristic freezing time has been defined as the time needed for a  
154 temperature change from the initial freezing point to a temperature at which 80% of the water  
155 has been converted to ice at a particular point. The time elapsed for a temperature change  
156 from  $-1$  to  $-7\text{ }^{\circ}\text{C}$  was considered as the characteristic freezing time, for apples and potatoes,  
157 based on literature (Delgado et al. 2009; Li & Sun, 2002). The overall freezing time in our  
158 study was defined as the time required for lowering the temperature of the geometrical centre  
159 of the product from the initial value of  $5\text{ }^{\circ}\text{C}$  to the target temperature of  $-18\text{ }^{\circ}\text{C}$ . The samples  
160 aimed for quality analyses followed exactly the same freezing procedures but without the  
161 insertion of the optical fibre. All the quality evaluation tests except cryo-SEM analysis were  
162 performed directly after the freezing process. The samples meant for cryo-SEM analysis were  
163 kept for 1 day at  $-80\text{ }^{\circ}\text{C}$  prior to imaging. Each experiment was performed at least in  
164 triplicates.

165

## 166 **2.3. Microstructure Analysis**

### 167 **2.3.1. X-rays micro-tomography**

168 This method has been extensively used to observe and visualize the structure of frozen  
169 products (in 2-D and 3-D) at ambient temperature after freeze-drying the samples (Mousavi,  
170 Miri, Cox, & Fryer, 2007; Ullah, Takhar, & Sablani, 2014; Zhao & Takhar, 2017). For X-ray  
171 micro-tomography analysis, the entire frozen samples were first dehydrated using a freeze-  
172 dryer for 24h (condenser temperature of  $-85\text{ }^{\circ}\text{C}$  and vacuum pressure of 5.33 Pa). The heat  
173 flux to the sample was restricted by wrapping the sample in aluminum foil; this strategy  
174 permitted to minimize any shrinkage of the sample during the freeze-drying process. The  
175 removal of the moisture inside the material by sublimation led to a network of solid fibers and  
176 pores. A residual moisture content of  $4 \pm 1\%$  (wet basis) measured in the samples after  
177 freeze-drying.

178 Afterwards, the freeze-dried samples were scanned by an X-ray micro-computed tomography  
179 scanner (SkyScan 1174v2, Bruker microCT, Kontich, Belgium) at a 50 kV voltage and 800  
180  $\mu\text{A}$  current. A CCD (charge-coupled device) camera with  $1,304 \times 1,024$  pixels resolution was  
181 used to record the projection images. The acquisition was performed at a voxel size of  $9\text{ }\mu\text{m}$   
182 (for apple) and  $13.5\text{ }\mu\text{m}$  (for potato). The exposure time was 1,600 ms, and the samples were  
183 rotated from  $0^{\circ}$  to  $180^{\circ}$  with a step angle of  $0.2^{\circ}$ . The average of three images per angular  
184 position was taken. A total of 923 images was acquired at the end of the process for each  
185 sample. Flat field correction was carried out to remove the artefacts that arose due to the  
186 variations in the pixel-to-pixel sensitivity of the detector and/or by distortions in the optical  
187 path.

188 Image processing comprised two steps, i.e. reconstruction and image analysis, in order to  
189 acquire the distribution characteristics of pores. 2-D images were reconstructed, using  
190 NRecon reconstruction software, from the series of images which were obtained during the  
191 image acquisition process, (Bruker microCT, Kontich, Belgium). The images comprising the  
192 entire sample were considered for the reconstruction process. Then, the alignment of the  
193 images with each other was corrected automatically. In the next step, the intensity range of the  
194 image was adjusted by its histogram, the lower limit of histogram was fixed at 0 and the upper  
195 limit was fixed as 0.068 (which was almost 20% higher than the maximum in the histogram  
196 for each case). The output image format was fixed as TIFF (16-bits), and upon reconstruction  
197 process, a series of images having a resolution of  $1,304 \times 1,304$  pixels was obtained.

198 The image analysis was performed using CTAN 1.16.4.1 image analysis software (Bruker  
199 microCT, Kontich, Belgium). The image on which 3-D analysis would be performed was  
200 initially selected and a stack of 750-800 slices images was selected for further processing. For  
201 all conditions, between 75 and 85 slices from the top and bottom were systematically removed  
202 due to their low quality and the region of interest (ROI) was defined. The ROI used for this  
203 study covered the sample entirely while excluding the information from the extreme periphery  
204 of the sample. The ROI represented roughly more than 80% of the raw image. The ROI was  
205 then thresholded (using automatic Otsu thresholding method) to separate the pixels into 2  
206 categories: the brightest (corresponding to the cellular matrix), and the darkest (corresponding  
207 to the pores). The resulting image, had only black and white pixels. Subsequently,  
208 despeckling was performed in order to remove from the image the floating pixels (generally  
209 due to noise) which are not attached to the main solid matrix. The pore distribution was  
210 measured directly in 3-D using the distance transform method described by Remy and Thiel  
211 (2002). The medial axes of all pores were determined using a “skeletonisation” process. The  
212 local thickness measurement was done for all voxels lying along this axis to obtain the pore  
213 size (or matrix size). The local thickness for a point in pores corresponded to the diameter of  
214 the largest sphere fulfilling two conditions:

- 215 (i) the sphere should encompass the point (the point should not be necessarily the centre  
216 of the sphere)
- 217 (ii) the sphere should be circumscribed by the pore boundary (or matrix boundary).

218

219 After the calculation of the pore size distribution and the mean pore size, the D-Values (D10,  
220 D50 and D90, the intercepts for 10%, 50% and 90% of the cumulative pore size distributions)  
221 were also calculated (Chevallier et al., 2014). For each freezing condition, at least three  
222 repetitions were done.

223

### 224 **2.3.2. Cryo-SEM analysis**

225 A very thin specimen (e.g. slab) was cut from the middle of the frozen apple samples using a  
226 sharp scalpel for cryo-SEM analysis. The specimen was fixed into the groove notched in a  
227 copper sample holder using an OCT (optimal cutting temperature) compound (Tissue-Tek,  
228 Sakura, Finetek, USA). The cutting operation was performed in cold condition (on a glass  
229 petri dish placed in a box filled with dry CO<sub>2</sub>) in order to avoid thawing of the sample. The  
230 sample remained for 2 min in a box filled with dry CO<sub>2</sub> to harden the OCT compound.

231 Afterwards, the sample was loaded onto a precooled copper specimen stub and was quickly  
232 transferred in the cryo-preparation chamber of cryo-SEM (LS10, ZEISS EVO, Germany)  
233 maintained under vacuum at  $- 80$  °C, where it was cryo-fractured using a precooled sharp  
234 knife mounted inside the chamber. The fractured sample was etched in the preparation  
235 chamber for about 10 min to expose the subsurface information. The sample was finally  
236 coated with a thin conducting layer of gold (5 nm) in the cryo-preparation chamber and then  
237 was transferred to the cold stage in the cryo-SEM (maintained at  $- 80$  °C) where  
238 microstructural observation was performed. The fractured surface of apples was examined  
239 with an accelerating voltage of 11 kV.

240

#### 241 **2.4.Texture analysis**

242 The frozen samples were thawed at room temperature ( $20 \pm 1$  °C) for 2 h in a zip-lock bag  
243 (“static air thawing” method) before performing colour, drip loss and texture measurements.

244 In our study, in order to determine the texture, the frozen apple and potato samples were  
245 thawed and compressed in a texture analyser (AMETEK, Lloyd Instruments, France) beyond  
246 the failure point which was marked by a significant drop in the force reading. A similar  
247 procedure was used by Khan & Vincent (1993, 1996) for determining the failure stress,  
248 Young’s modulus, and failure strain of apple and potato. Based on our preliminary trials and  
249 results from Khan & Vincent (1993) and Alvarez, et al. (2002), compression of the sample to  
250 50% strain was found more than sufficient to cause the failure of the sample. The maximum  
251 force exerted during the compression test was recorded as the firmness/hardness (N) of the  
252 samples. For apple firmness measurement, the other test parameters like the load cell, the  
253 operating test speed and the diameter of the circular compression plate were 50 N, 100  
254 mm/min and 21 mm, respectively. These parameters in the case of potatoes were 1000 N, 50  
255 mm/min and 50 mm. The stress vs. strain curves during compression tests were further  
256 examined and Young’s modulus (E) (the slope of the loading curve at the point of its highest  
257 gradient) was acquired for potato (Chassagne-Berces et al., 2009). The Young’s modulus  
258 measurements were only performed for potatoes. The test parameters for Young’s modulus  
259 and firmness determination of potato were the same. All measurements were performed at  
260  $21 \pm 2$  °C. At least 12 samples were analyzed for each freezing condition.

261

#### 262 **2.5. Drip loss**

263 The drip loss was determined on the basis of weight difference between frozen sample (W1),  
264 and thawed sample (W2). The drip loss (%) was calculated using Eq. (1). To prevent

265 condensation of moisture, the sample was maintained in a sealed pouch until complete  
266 thawing.

$$\text{Drip Loss (\%)} = \frac{W_1 - W_2}{W_1} \times 100 \quad (1)$$

## 267 **2.6. Colour analysis**

268 The colour of the potatoes was measured using a portable and handheld chroma meter CR-  
269 400 (Konica Minolta, Inc. Japan). Using this equipment, the  $L^*$ ,  $a^*$ ,  $b^*$  values of the samples  
270 were obtained with high accuracy (precision of  $L^*$ ,  $a^*$ ,  $b^*$  values were  $\pm 0.02\%$ ,  $\pm 0.21\%$  and  
271  $\pm 0.15\%$ , respectively). The maximum value for  $L^*$  is 100 (represents a perfectly white surface  
272 or a perfectly reflecting diffuser) and its minimum value is 0 (represents perfectly black  
273 surface). The positive and negative  $a^*$  correspond to red and green colour. Similarly, positive  
274 and negative  $b^*$  represent yellow and blue colour, respectively.

275 A single value for the colour difference was achieved by calculating the overall colour  
276 difference ( $\Delta E$ ) value; it takes into account the differences between  $L^*$ ,  $a^*$ ,  $b^*$  of the specimen  
277 (e.g. frozen-thawed sample) and reference (fresh sample), and is obtained using Eq. (2)  
278 (Anon, 2018). The frozen samples were thawed prior to the colour measurements. At least  
279 eight measurements were recorded for each freezing protocol.

$$\Delta E = \sqrt{\Delta L^{*2} + \Delta a^{*2} + \Delta b^{*2}} \quad (2)$$

## 280 **2.7. Estimation of freezable water and total water content**

281 The latent heat corresponding to the ice–water transition in the matrices was determined using  
282 a  $\mu$ DSC 7 EVO DSC (Setaram, Caluire, France) device connected to a cooling bath. The  
283 initial temperature in the cell was  $-35\text{ }^\circ\text{C}$  and a scan at  $1\text{ }^\circ\text{C}/\text{min}$  was programmed up to a  
284 final temperature of  $20\text{ }^\circ\text{C}$ . 10 min dwell isotherms were programmed at the initial and the  
285 final temperatures. The reference cell was an empty cell similar to the one containing the  
286 apple and potatoes samples. The samples of the matrices were weighed (80–150 mg) in the  
287 sample's DSC cell. The programming and the elaboration of the spectra were performed with  
288 Data Acquisition (version 4.1D — TA Instruments) and Calisto Processing (version 1.065 —  
289 Setaram, Caluire, France) software packages. The measurement of the matrices dry matter  
290 was carried out with the dehydration of pre-weighed samples for 24 h in an oven tuned at  $104$   
291  $^\circ\text{C}$ . The results were acquired as an average of 10 repetitions from different apples and  
292 potatoes of each batch. The percentage of freezable water (FW (%)) was calculated using the  
293 area of the integrated endothermic peak at the range of  $0\text{ }^\circ\text{C}$ . The endothermic peak arises

294 from the phase transition of ice into water. Eq. (3) was used in order for the freezable water of  
295 the matrices to be estimated.

$$\text{FW (\%)} = \frac{Q \cdot 100}{H_f \cdot m_s} \quad (3)$$

296

297 FW (%) is the percentage of freezable water, Q is the enthalpy (J),  $H_f$  represents the heat of  
298 fusion ice–water equal to  $333.50 \text{ J} \cdot \text{g}^{-1}$  of ice/water and  $m_s$  is the mass of the sample (g).

299

## 300 **2.8. Statistical Analysis**

301 One-way ANOVA (Analysis of variance) was used to determine any significant differences  
302 among the trials associated with the analyzed parameters. Duncan's multiple range test was  
303 performed to determine differences of means ( $p < 0.05$ ).

304

## 305 **3. Results**

### 306 **3.1. MAF of apples**

307 Further than the conventional freezing (in the absence of MW), freezing of apples under  
308 pulsed power MAF conditions such as P1MAF (10 s /500 W/kg – 20 s /0 W/kg) and P2MAF  
309 (10 s /667 W/kg – 20 s /0 W/kg), constant power MAF condition (CMAF = 167 W/kg) was  
310 performed. In this section, the results (in terms of freezing and quality parameters) obtained  
311 for freezing of apples under the aforementioned freezing conditions will be presented and  
312 discussed.

313

#### 314 **3.1.1. Effect of MAF on freezing process of apple**

315 The pattern of the freezing curves obtained during conventional freezing and MAF of apples  
316 were very similar to each other (Figure 1). The temperature measurements showed no  
317 significant differences between the freezing point temperature among the different conditions.  
318 The freezing point temperatures for control, CMAF, P1MAF and P2MAF conditions were  
319  $-2.78 \pm 0.43 \text{ }^\circ\text{C}$ ,  $-2.70 \pm 0.10 \text{ }^\circ\text{C}$ ,  $-2.60 \pm 0.51 \text{ }^\circ\text{C}$  and  $-2.57 \pm 0.37 \text{ }^\circ\text{C}$ , respectively.  
320 Slight temperature fluctuation was observed during the phase transition period for pulsed  
321 MAF conditions, while no such fluctuations were observed for control and CMAF conditions.  
322 Differences (in terms of temperature fluctuation) between CMAF and PMAF conditions may  
323 be due to the power level and the emitted pulse shape used during the respective processes.  
324 Xanthakis et al. (2014) reported similar temperature fluctuations during their PMAF

325 conditions, however, the magnitude of temperature fluctuations in the present case was lower  
326 (ca. 0.1-0.2°C amplitude) due to lower power level. Although the observed oscillations were  
327 quite small, they were matching with the duty ratio in terms of timing, which confirms that  
328 those temperature oscillations were related with instant heating due to the emitted MW power.  
329 Another difference between the two studies was the used mode of freezing. Xanthakis et al.  
330 (2014) used unidirectional freezing, while in this study multidirectional freezing occurred  
331 through turbulent cold air which generated greater heat flux. The temperature fluctuation  
332 intensity during MAF was also dependent on the temperature drop during each step of MW  
333 emission tranquility between two sequential pulses. In this study, the heat generated during  
334 MW exposure was rapidly removed due to higher the heat flux than in the case of Xanthakis  
335 et al. (2014), thus leading to less intense temperature oscillation peaks. The representative  
336 time-temperature profiles demonstrated that the application of MWs during the freezing  
337 process had no significant impact on the overall freezing time. The characteristic freezing  
338 times for all the tested conditions were not significantly different from each other (Table 1).  
339 The current findings are in accordance with Hafezparast-Moadab et al. (2018) who found that  
340 the application of RF during the freezing of fish matrices did not affect the shape of the  
341 freezing curve and the total freezing time. Xanthakis et al. (2014) observed lower freezing  
342 rate and thus longer freezing time during MAF freezing of pork meat under different MW  
343 power levels. It is worth mentioning that the freezing time during MAF of food further than  
344 the power of MWs also depends on the surface to volume ratio (S/V) of the food product as  
345 well as on the mode of freezing (unidirectional or multidirectional). The greater S/V along  
346 with the existence of no thermal gradient might have aided in quicker dissipation of heat  
347 generated during MW exposure which in turn, may have prevented an increase in the  
348 characteristic freezing time. These results indicated that together with the heat flux, S/V of the  
349 product may affect the characteristic freezing time during MAF of food.

350

### 351 **3.1.2. X-ray tomography of frozen apple**

352 The pore size distributions for each freezing condition obtained by using X-ray micro-  
353 tomography are presented in Figure 2a. It can be mentioned that MAF conditions led to  
354 improved microstructure (smaller pores and more homogeneous structure) than the control  
355 condition. The mean pore sizes obtained are presented in Table 1. The samples frozen in the  
356 absence of MW exposure had the largest mean pore size ( $151.76 \pm 7.45 \mu\text{m}$ ), while, the  
357 P2MAF condition showed the smallest mean pore size in the case of apples  
358 ( $127.63 \pm 4.63 \mu\text{m}$ ). The order of the mean pore size obtained under the tested conditions was

359 control freezing > CMAF > P1MAF > P2MAF. The statistical analysis of mean pore size  
360 depicted that PMAF conditions significantly reduced the pore size in apple compared to the  
361 control condition. Meanwhile, mean pore size under CMAF condition were not significantly  
362 different compared with the control and PMAF conditions. The MW emission form and  
363 power level were found to govern the pore size distribution in the apple sample, since the  
364 mean pore size decreased significantly ( $p < 0.05$ ) with the introduction of MW pulsed  
365 conditions and with the increase in MW power compared with the control.

366 For a better understanding of pore size distribution, the cumulative pore size distribution  
367 (Figure 2b) and the D-Values (D10, D50 and D90 values, the intercepts for 10%, 50% and  
368 90% of the cumulative pore size distributions) were also calculated (Table 1). The cumulative  
369 pore size distribution indicates that the control condition resulted in relatively larger pore  
370 throughout the distribution range than the MAF conditions (Figure 2b). For instance, the  
371 control had the largest D10, D50 and D90 values i.e.  $62.53 \pm 3.27$ ,  $137.59 \pm 5.86$  and  
372  $227.21 \pm 13.85 \mu\text{m}$ , while these values were relatively lower in apple frozen under MAF  
373 conditions (Table 1). The D-Values (D10, D50 and D90 values) for P2MAF condition were  
374 significantly smaller than those of the control freezing conditions. The D50 and D90 value for  
375 P1MAF was significantly smaller than the control, while, D10 value for P1MAF and control  
376 freezing conditions were not significantly different from each other. Among MAF conditions,  
377 no significant difference in D-Values were observed. According to these results, it can be  
378 mentioned that upon increasing the power level of MW, the amount of large size pores  
379 decreased and at the same time amount of the smaller pores increased.

380

### 381 **3.1.3 Cryo-SEM analysis of frozen apple**

382 Cryo-SEM was also performed for apple samples frozen under control and different MAF  
383 conditions (Figure 3). The bright regions in the micrographs (in Figure 3b-e) are the solidified  
384 solutes of the cell sap, the cytoplasmic membrane and the cell walls. The darker regions in the  
385 micrographs are ice (majorly inside the cell-“intracellular ice”); some dark regions (indicated  
386 by letter A in the Figure 3b-e are the air space between the cells). Upon analyzing the  
387 microstructure morphology, it was found that all of the freezing conditions maintained cell  
388 structure when compared to the structure of the fresh sample (Figure 3a). However, the  
389 freezing conditions had an effect on the inner morphology of the cell since the size of ice  
390 crystals was influenced. The control freezing condition had the most detrimental effect on the  
391 inner morphology of the cell as relatively bigger ice crystals were formed compared to the  
392 MW assisted frozen samples. Moreover, control freezing led to a non-homogenous inner

393 structure compared to the MAF conditions. Furthermore, the control sample had a few larger  
394 ice crystals, while no such large crystals were observed under the different MAF conditions.  
395 Concerning the different MAF conditions, CMAF led to bigger ice crystals compared to  
396 PMAF conditions, while, P2MAF resulted in the smallest formed ice crystals among all  
397 conditions. Unfortunately, calculations for ice crystals size were not performed as it was  
398 difficult to locate the boundary of the ice crystals. The ice crystals had a 3D structure and  
399 even though the calculations were made, we could get only 2D information. Ultimately, this  
400 would have led to an inaccurate estimation of the size of the ice crystals. Although  
401 quantitative analysis of the ice crystals size could not be performed, the micrographs obtained  
402 (using cryo-SEM) showed indicative differences between the different processing conditions.  
403 These results are in accordance with Xanthakis et al. (2014) and Sadot et al. (2018) who  
404 reported that the application of MWs (2.45 GHz) during freezing yielded a better  
405 microstructure (in terms of reduced ice crystals size) in both real and model food systems  
406 (pork tenderloin and methylcellulose gel) than the control condition. Furthermore, Xanthakis  
407 et al. (2014) found that the mean ice crystal size in the pork meat decreased with the  
408 increasing power level of applied MW. A similar trend was found in our study, since the  
409 increase in MW power level decreased the mean size of ice crystals in apple. These results  
410 showed similarities with those obtained from studies on freezing of meat and fish matrices  
411 under the influence of RF waves, (Anese et al., 2012; Hafezparast-Moadab et al., 2018) which  
412 proposed that RF exposure during freezing reduced the size of ice crystals in the product.  
413 Two concepts can be proposed to explain the observed ice crystal size reduction in MAF  
414 frozen systems. The “NITOM” concept (Nucleation Induced by Temperature Oscillation  
415 caused by MWs) which is based on the fact that under specific duty ratio, the temperature of  
416 the sample undergoing freezing will oscillate (Xanthakis et al., 2014). The fluctuating  
417 temperature is expected to favour secondary nucleation which in turn suppresses the crystal  
418 growth. The second concept is called “NIMIW” (Nucleation Induced by constant or pulsed  
419 MicroWave power) and it is based on constant or pulsed (short time) emission. NIMIW can  
420 be explained by the impact of MW radiation on the hydrogen bonds between water molecules,  
421 which may affect the water cluster structures during freezing. It is expected that MWs would  
422 exert a torque and displace the water molecules from their equilibrium relationships in the ice  
423 cluster resulting in fragmentation of existing ice crystals when ice crystals are in the form of  
424 nuclei. The fragmented ice crystals nuclei may act as new nucleation sites and promote the  
425 secondary nucleation, thus, causing ice crystal size reduction (Hanyu et al., 1992; Jackson et  
426 al., 1997; Anese et al., 2012; Xanthakis et al., 2014; Dalvi-Isfahan et al., 2016; Cheng et al.,

427 2017). Another possibility could be that the electrical disturbances caused by MW application  
428 would alter the mass diffusion in the quasi-liquid layer surrounding the ice crystals under  
429 formation (Fletcher, 1970). The delayed growth of ice crystals would, in turn, yield a higher  
430 nucleation rate resulting in a refinement of the size of ice crystals in the product (Hanyu et al.,  
431 1992; Jackson et al., 1997; Anese et al., 2012; Dalvi-Isfahan et al., 2016, Hafezparast-Moadab  
432 et al. 2018). The two described hypotheses, NITOM and NIMIW may be considered to  
433 explain the mechanism of action of the observed reduction of ice crystals size in MAF frozen  
434 apples.

435

### 436 **3.1.4 Texture of frozen apple**

437 The firmness values of apples under different freezing conditions are presented in Figure 3f.  
438 The firmness of fresh apple was  $13.23 \pm 1.56$  N, and it was significantly reduced ( $p < 0.05$ )  
439 after freezing and thawing. The firmness value was slightly better retained under P2MAF  
440 ( $5.59 \pm 0.91$  N) and P1MAF ( $5.11 \pm 0.89$  N) conditions compared with those of the control  
441 ( $4.57 \pm 0.92$  N) and CMAF ( $4.64 \pm 0.87$  N) conditions (Figure 3f). The firmness value was  
442 slightly higher when the applied MWs were in pulsed form and had a higher power level. The  
443 firmness/hardness of frozen-thawed product is linked to the size of ice crystals formed in the  
444 product. It is well known that the formation of small size ice crystals causes less damage to  
445 the microstructure and hence less texture degradation compared to large ice crystals formed in  
446 a food matrix (Chassagne-Berces et al., 2009; Chassagne-berces, Fonseca, Citeau, & Marin,  
447 2010; Jha et al., 2018; Mazur, 1984). The results shown in Figure 2 and Figure 3b-e indicate  
448 that MAF process reduced the average size of ice crystals in the product and this, in turn,  
449 might have caused less damage (both mechanical and biochemical damage), resulting in  
450 improved texture preservation than the control sample. Hafezparast-Moadab et al. (2018) and  
451 Anese et al., (2012) reported that RF assisted freezing process causes less texture damage  
452 compared to conventional freezing.

453

### 454 **3.1.5 Drip loss of frozen apple**

455 Figure 3g shows the effect of MAF on drip loss. Compared to the control sample, the drip loss  
456 value decreased approximately 3, 23 and 42% under CMAF, P1MAF and P2MAF conditions,  
457 respectively. However, only P2MAF condition led to a significant reduction ( $p < 0.05$ ) in drip  
458 loss. These results are coherent with microstructure and texture loss results mentioned above.  
459 The drip loss (especially from frozen fruits and vegetables) depends on the size and location  
460 of ice crystals in the food as well as on the thawing rate (Van Buggenhout et al., 2006;

461 Zaritzky, 2000). In our study, since the thawing rate was kept constant for all the trials, the  
462 drip loss can be attributed to the ice crystal size and location. Higher drip loss in the case of  
463 control sample can be related to the increased mean ice crystal size in the product. It has been  
464 confirmed in several studies that the genesis of larger ice crystals lead to higher drip loss due  
465 to (i) higher destruction of cellular structure resulted by mechanical, chemical and shrinkage  
466 effects (Bevilacqua, Zaritzky, & Calvelo, 1979; Delgado & Sun, 2001; Sadot, Curet, Rouaud,  
467 Le-bail, & Havet, 2017) and (ii) lower re-absorption of water during thawing; bigger ice  
468 crystals have a smaller specific surface area leading to reduced water re-absorption during  
469 thawing (Bevilacqua et al., 1979; Sadot et al., 2017). Freezing using electromagnetic waves in  
470 the RF frequency range (27.12 MHz) has also resulted in lower drip loss for meat and fish  
471 matrices (Anese et al., 2012; Hafezparast-Moadab et al., 2018).

472

### 473 **3.2. MAF of potatoes**

474 Based on the results acquired from apple freezing under control and MAF conditions and also  
475 from previous studies (Xanthakis et al., 2014; Anese et al., 2012; Hafezparast-Moadab et al.  
476 2018), it can be inferred that electromagnetic radiation in pulsed mode may have a greater  
477 potential for disturbing the crystallization of water contained in food products. In all these  
478 cases the ice crystal size was reduced resulting in frozen products with improved quality  
479 characteristics. Considering this fact, freezing trials of potatoes were performed only under  
480 PMAF conditions and were compared with the control conditions.

481

#### 482 **3.2.1. Effect of MAF on freezing process of potato**

483 The time-temperature histories during control and MAF processes exhibited similar shape  
484 irrespective of the used freezing conditions (Figure 4a). No supercooling was observed for  
485 any of the freezing conditions. The initial freezing point for control, P1MAF and P2MAF  
486 conditions were recorded as  $-0.75 \pm 0.23$  °C,  $-0.70 \pm 0.29$  °C and  $-0.90 \pm 0.14$  °C,  
487 respectively. These values indicated that the MAF processes did not have any effect on the  
488 initial freezing point of the potatoes. Temperature fluctuation was observed during the phase  
489 transition period for pulsed MAF conditions, while no such fluctuations were observed for  
490 control condition. The magnitude of temperature fluctuation was slightly larger than for apple.  
491 The characteristic freezing time and overall freezing time increased slightly while the overall  
492 freezing rate showed a decreasing trend upon the application of MWs as well as with the  
493 increasing power level of MWs (Table 1). These differences were found to be insignificant.  
494 No significant differences in the freezing curve characteristics between control and MAF

495 conditions can be related to blanching pretreatment and the freezing conditions which were  
496 used for these tests. The blanching process might have caused partial breakdown of the  
497 cellular structure, leading to an enhanced heat transfer during the freezing process. It has been  
498 reported that intact cellular structure impedes heat transfer, while any sort of alteration (like  
499 poration or breakdown of cellular structure) can allow a better heat transfer (Li, Zhu, & Sun,  
500 2018). Similarly, the higher airflow rate used for these experiments (i.e. 2.3-2.5 m/s air  
501 velocity used for these tests instead of 1.1 m/s for the previous tests with apple) might have  
502 improved the convective heat transfer coefficient around the sample and increase heat  
503 transfer. The increase in heat transfer rate due to blanching treatment and the higher airflow  
504 rate might have compensated for the heat that could have generated due to MW application,  
505 resulting in no significant increase in the total freezing time.

506

### 507 **3.2.2. X-ray micro-tomography of frozen potato**

508 The size distributions of the formed ice crystals during control and MAF conditions were  
509 quantified using X-ray micro-tomography. The pores created within the matrix during the  
510 freeze-drying of frozen potatoes have been referred as the footprint of the ice crystals by  
511 Ullah et al. (2014) Zhao & Takhar (2017). Figure 4b, c illustrates the pore size distribution  
512 under control and MAF conditions. It is evident from those results that P2MAF condition led  
513 to smaller pores than the samples frozen under P1MAF and control conditions. Control  
514 condition not only formed relatively larger pore size but also had a broader distribution range  
515 than those of the MAF conditions. Since the pore distributions range under MAF conditions  
516 were narrower, the formed pores were more uniform in size than those of the control samples.  
517 The mean pore size obtained for each freezing condition is shown in Table 1. Compared to the  
518 control samples, P1MAF and P2MAF conditions reduced the mean pore size by 22.20% and  
519 18.91% respectively. The difference in mean pore size was significant ( $p < 0.05$ ) between the  
520 control and P2MAF conditions. The pore size formed under P1MAF condition was not  
521 significantly different than those formed under P2MAF and control conditions. Furthermore,  
522 the cumulative pore size distributions were plotted and the D-Values (D10, D50 and D90)  
523 were also calculated for in-depth understanding of pore size distribution in the product (Figure  
524 4b and Table 1). The D10 value could only be calculated for the control condition, while it  
525 was not possible to obtain D10 values for PMAF conditions due to resolution limitation (i.e.  
526 voxel size of 13.5  $\mu\text{m}$ ). Using this voxel size the minimum pore size that could be detected  
527 was 27  $\mu\text{m}$ . In the case of MAF conditions, it was observed that pore below 27  $\mu\text{m}$  accounted  
528 more than 10% on an average basis. Since the calculation of D10 value required two points

529 one representing the value below 10% and other representing a value above 10%, the lack of a  
530 value below 10% in the case of MAF conditions made it difficult to calculate the D10 value.  
531 The median D50 values of pores under P1MAF and P2MAF conditions were 22.36% ( $p >$   
532 0.05) and almost 30% ( $p < 0.05$ ) smaller than that obtained after freezing under control  
533 condition. The D90 values of pores exhibited similar trend as mean and median pore size for  
534 the studied conditions (Table 1). From these findings, it can be indicated that freezing under  
535 MAF condition led to the formation of smaller ice crystals showing a narrow range of  
536 distribution, in which in turn gave a product having more homogenous structure than the  
537 control sample. These results showed similar trend with the results obtained during MAF of  
538 apples. Although the different tested matrices and the modified freezing equipment, MAF  
539 frozen potatoes showed ice crystal size reduction, like apple samples, compared to the  
540 corresponded control samples. Both hypotheses, NITOM and NIMIW may also be  
541 responsible for the reduction of ice crystals size mechanism in MAF of potatoes.

542

### 543 **3.2.3 Texture and drip loss of frozen potato**

544 Figure 5a and b represents the hardness and Young's modulus of the potatoes at different  
545 processing steps. The hardness and Young's modulus values of the fresh potato were the  
546 highest averaging  $189.94 \pm 18.80$  N and  $5.46 \pm 0.44$  MPa. Blanching process reduced both  
547 the hardness and Young's modulus values (approx. by 17%). The blanching process causes  
548 thermal destruction of cell membranes and hence tissue loses its turgor pressure and rigidity  
549 resulting in softening of tissues (Reid et al., 1986; Reis, 2017; Verlinden et al., 2000). The  
550 blanched frozen-thawed potatoes were found to be softer than both the fresh and blanched  
551 samples. The hardness of fresh potatoes, after blanching and subsequent freezing-thawing  
552 degraded by approximately 88%, 89% and 90% under P2MAF, P1MAF and control freezing  
553 conditions. Young's modulus value showed similar trend as it was decreased by  
554 approximately 86%, 89% and 91% under P2MAF, P1MAF and control freezing conditions  
555 respectively, compared to the fresh samples.

556 The drip loss data acquired for control and MAF samples are shown in Figure 5c. Freezing  
557 under control freezing condition resulted in higher drip loss ( $2.67 \pm 1.12$  %) compared to all  
558 the tested MAF conditions (P1MAF:  $2.03 \pm 0.88$  % ( $p > 0.05$ ) and P2MAF:  $1.62 \pm 0.70$  % ( $p$   
559  $< 0.05$ )). The reasons behind the better texture preservation and water holding capacity of  
560 potatoes under MAF conditions can be explained in similar manner as in the section 3.1.4 and  
561 3.1.5 for the case of frozen apples.

562

### 563 **3.2.4 Colour evaluation of frozen potato**

564 The colour of fresh, blanched, and blanched-frozen-thawed potato are represented in Figure  
565 5d. The blanching process did not affect  $L^*$  (lightness) value but it decreased the  $b^*$   
566 (yellowness) value and imparted negative  $a^*$  (green) value compared to fresh samples. The  
567 freezing-thawing process of blanched sample did not affect the colour characteristics.  
568 Moreover, none of the freezing protocols caused any further significant effect to the colour  
569 characteristics of the blanched potato. The colour change in unblanched potatoes upon  
570 freezing-thawing is mainly associated with the browning that generally happens due to  
571 enzymatic activity during the thawing process (Cano, 1996; Koch et al., 1996). In our study,  
572 the blanching process seems that inactivated efficiently the enzymes and prevented from any  
573 colour change upon freezing and subsequent thawing.

574

### 575 **4. Conclusions**

576 MAF and conventional freezing of apples and potatoes were performed and evaluated with  
577 respect to microstructural characteristics and quality attributes. MAF experiments were  
578 carried out by means of a custom-built MW freezer, which consisted of a specially modified  
579 domestic MW cavity connected to a MW solid state emitter and installed in a blast freezer. To  
580 the best of our knowledge, this is the first time that a MAF process is used for freezing plant  
581 based products such as apples and potatoes. In this study, the impact of MAF conditions on  
582 freezing parameters and quality attributes (for e.g. microstructure, texture, drip loss, etc.) of  
583 apples and potatoes were studied using several analytical techniques.

584 In the case of apple, the application of MW use during freezing did not affect the freezing  
585 parameters. The shapes of the obtained freezing curves during conventional freezing and  
586 MAF of apples were almost identical to each other. No supercooling was observed for any of  
587 the freezing conditions. The characteristic freezing time, the overall freezing time and the  
588 freezing rate values were found to be similar for all conditions. Concerning quality  
589 parameters, the application of MWs during freezing process resulted in more homogenous  
590 pore size distributions with larger populations of small pores than the control samples.  
591 Moreover, MAF of apple resulted in a lower drip loss, meanwhile, it also retained better the  
592 firmness/hardness compared to the reference sample. The MW form (constant mode or pulsed  
593 mode) and power level were found to be critical parameters for the quality attributes of final  
594 frozen apple sample. Pulsed conditions with the higher tested MW power (P2MAF) gave the  
595 best results in terms of microstructure and other quality attributes such as drip loss and  
596 texture.

597 The application of pulsed MAF to potato samples showed similar trends with those for apple.  
598 The freezing curve shapes and the freezing parameters (characteristic freezing time, the  
599 overall freezing time and freezing rate) were unaffected by the introduction of the MW during  
600 freezing of potato. The MAF samples exhibited microstructure with smaller pores and more  
601 uniform size distributions compared to the control sample. The texture and the drip loss were  
602 also improved for MAF samples compared to the control sample. No significant impact of any  
603 of the tested freezing conditions on the colour parameters was observed. The quality  
604 preservation was greater when MW intensity was increased. Among all freezing conditions,  
605 P2MAF condition yielded in improved microstructure and other quality attributes such as drip  
606 loss and texture.

607 Two concepts namely “NITOM” and “NIMIW” have been proposed to explain the observed  
608 ice crystal size reduction in MAF samples. This study demonstrated that MW assisted  
609 freezing can improve the freezing of more sensitive cellular food matrices such as fruits and  
610 vegetables by reducing the ice crystal size and retain better the quality attributes compared to  
611 conventional freezing.

612

### 613 **Acknowledgments**

614 This work received financial support from ONIRIS, the French National Research Agency  
615 (ANR) and the Swedish Research Council FORMAS, under the FREEZEWAVE project  
616 (SUSFOOD - ERANET, FR: ANR-14-SUSF-0001, SE: 2014-1925).

617 **Reference**

618

619 Alvarez, M. D., Canet, W., & López, M. E. (2002). Influence of deformation rate and degree  
620 of compression on textural parameters of potato and apple tissues in texture profile  
621 analysis. *European Food Research and Technology*, 215(1), 13–20.

622 Anese, M., Manzocco, L., Panozzo, A., Beraldo, P., Foschia, M., & Nicoli, M. C. (2012).  
623 Effect of radiofrequency assisted freezing on meat microstructure and quality. *Food*  
624 *Research International*, 46(1), 50–54.

625 Anon (2018). <http://cobra.rdsor.ro/cursuri/cielab.pdf>. Retrieved on 3<sup>rd</sup> July 2018.

626 Bevilacqua, A., Zaritzky, N. E., & Calvelo, A. (1979). Histological measurements of ice in  
627 frozen beef. *Journal of Food Technology*, 14, 237–251.

628 Cano, M. P. (1996). Vegetables. In L. E. Jeremiah (Ed.), *Freezing effects on food quality* (pp.  
629 247–298). New York: Marcel- Dekker.Inc.

630 Chassagne-berces, S., Fonseca, F., Citeau, M., & Marin, M. (2010). Freezing protocol effect  
631 on quality properties of fruit tissue according to the fruit , the variety and the stage of  
632 maturity. *LWT - Food Science and Technology*, 43, 1441–1449.

633 Chassagne-Berces, S., Poirier, C., Devaux, M. F., Fonseca, F., Lahaye, M., Pigorini, G.,  
634 Girault, C., Marin, M., & Guillon, F. (2009). Changes in texture, cellular structure and  
635 cell wall composition in apple tissue as a result of freezing. *Food Research International*,  
636 42, 788–797.

637 Cheng, L., Sun, D. W., Zhu, Z., & Zhang, Z. (2017). Emerging Techniques for Assisting and  
638 Accelerating Food Freezing Processes—A Review of Recent Research Progresses.  
639 *Critical Reviews in Food Science and Nutrition*, 57(4), 769–781.

640 Chevallier, S., Réguerre, A., Bail, A. Le, & Valle, G. Della. (2014). Determining the Cellular  
641 Structure of Two Cereal Food Foams by X-ray Micro-Tomography. *Food Biophysics*, 9,  
642 219–228.

643 Dalvi-Isfahan, M., Hamdami, N., Xanthakis, E., & Le-Bail, A. (2016). Review on the Control  
644 of Ice Nucleation by Ultrasound Waves, Electric and Magnetic Fields. *Journal of Food*  
645 *Engineering*, 195, 222–234.

646 Delgado, A. E., & Sun, D.-W. (2001). Heat and mass transfer models for predicting freezing  
647 processes – a review. *Journal of Food Engineering*, 47(3), 157–174.

648 Delgado, A. E., Zheng, L., & Sun, D. W. (2009). Influence of ultrasound on freezing rate of  
649 immersion-frozen apples. *Food and Bioprocess Technology*, 2(3), 263–270.

650 Hafezparast-Moadab, N., Hamdami, N., Dalvi-Isfahan, M., & Farahnaky, A. (2018). Effects

651 of radiofrequency-assisted freezing on microstructure and quality of rainbow trout  
652 (Oncorhynchus mykiss) fillet. *Innovative Food Science and Emerging Technologies*.

653 Hanyu, Y., Ichikawa, M., & Matsumoto, G. (1992). An improved cryofixation method:  
654 cryoquenching of small tissue blocks during microwave irradiation. *Journal of*  
655 *Microscopy*, 165(2), 255–271.

656 Jackson, T. H., Urgan, A., Critser, J. K., & Gao, D. (1997). Novel microwave technology for  
657 cryopreservation of biomaterials by suppression of apparent ice formation. *Cryobiology*,  
658 34(4), 363–372.

659 Jha, P. K., Xanthakis, E., Chevallier, S., Jury, V., & Le-Bail, A. (2018). Assessment of freeze  
660 damage in fruits and vegetables. *Food Research International*. In press, accepted article.

661 Khan, A. A., & Vincent, J. F. V. (1993). Compressive Stiffness and Fracture Properties of  
662 Apple and Potato Parenchyma. *Journal of Texture Studies*, 24, 423–435.

663 Khan, A. A., & Vincent, J. F. V. (1996). Mechanical damage induced by controlled freezing  
664 in apple and potato. *Journal of Texture Studies*, 27(1996), 143–157.

665 Koch, H., Seyderhelm, I., Wille, P., Kalichevsky, M. T., & Knorr, D. (1996). Pressure-shift  
666 freezing and its influence on texture, colour, microstructure and rehydration behaviour of  
667 potato cubes. *Molecular Nutrition & Food Research*, 40(3), 125–131.

668 Li, B., & Sun, D.-W. (2002). Effect of power ultrasound on freezing rate during immersion  
669 freezing of potatoes. *Journal of Food Engineering*, 55(3), 277–282.

670 Li, D., Zhu, Z., & Sun, D.-W. (2018). Effects of freezing on cell structure of fresh cellular  
671 food materials : A review. *Trends in Food Science & Technolog*, 75, 46–55.

672 Mazur, P. (1984). Freezing of living cells: mechanisms and implications. *American Journal of*  
673 *Physiology–Cell Physiology*, 247, C125–142.

674 Mousavi, R., Miri, T., Cox, P. W., & Fryer, P. J. (2007). Imaging food freezing using X-ray  
675 microtomography. *International Journal of Food Science and Technology*, 42(6), 714–  
676 727.

677 Reid, D. S., Carr, J. M., Sajjaanantakul, T., & Labavitch, J. M. (1986). Effects of Freezing and  
678 Frozen Storage on the Characteristics of Pectin Extracted from Cell Walls. In *Chemistry*  
679 *and Function of Pectins* (Symposium, Vol. 310, pp. 200–216). Washington, DC:  
680 American Chemical Society.

681 Reis, F. R. (Ed.). (2017). *New Perspectives on Food Blanching*. Cham: Springer International  
682 Publishing Switzerland.

683 Remy, E., & Thiel, E. (2002). Medial axis for chamfer distances: Computing look-up tables  
684 and neighbourhoods in 2D or 3D. *Pattern Recognition Letters*, 23, 649–661.

- 685 Sadot, M., Curet, S., Rouaud, O., Le-bail, A., & Havet, M. (2017). Numerical modelling of an  
686 innovative microwave assisted freezing process. *International Journal of Refrigeration*,  
687 80, 66–76.
- 688 Sadot, Mathieu & Curet, Sebastien & Rouaud, Olivier & Le Bail, Alain & Havet, Michel.  
689 (2018). Bénéfices d'une assistance micro-ondes sur la qualité de la congélation. *Revue*  
690 *Générale du Froid & du conditionnement d'air*, 25-32.
- 691 Shi, X., Datta, A. K., & Mukherjee, Y. (1998). Thermal Stresses From Large Volumetric  
692 Expansion During Freezing of Biomaterials. *Transactions of the ASME*, 120, 720–726.
- 693 Shi, X., Datta, A. K., & Mukherjee, Y. (1999). Thermal fracture in a biomaterial during rapid  
694 freezing. *Journal of Thermal Stresses*, 22, 275–292.
- 695 Shi, X., Datta, A. K., & Throop, J. A. (1998). Mechanical Property Changes during Freezing  
696 of a Biomaterial. *Transactions of the ASAE*, 41, 1407–1414.
- 697 Sun, D. W., & Li, B. (2003). Microstructural change of potato tissues frozen by ultrasound-  
698 assisted immersion freezing. *Journal of Food Engineering*, 57(4), 337–345.
- 699 Ullah, J., Takhar, P. S., & Sablani, S. S. (2014). Effect of temperature fluctuations on ice-  
700 crystal growth in frozen potatoes during storage. *LWT - Food Science and Technology*,  
701 59(2), 1186–1190.
- 702 Van Buggenhout, S., Messagie, I., Maes, V., Duvetter, T., Loey, A. Van, & Hendrickx, M.  
703 (2006). Minimizing texture loss of frozen strawberries: effect of infusion with  
704 pectinmethylesterase and calcium combined with different freezing conditions and effect  
705 of subsequent storage / thawing conditions. *European Food Research and Technology*,  
706 223, 395–404.
- 707 Verlinden, B. E., Yuksel, D., Baheri, M., De Baerdemaeker, J., & Van Dijk, C. (2000). Low  
708 temperature blanching effect on the changes in mechanical properties during subsequent  
709 cooking of three potato cultivars. *International Journal of Food Science and Technology*,  
710 35, 331–340.
- 711 Xanthakis, E., Havet, M., Chevallier, S., Abadie, J., & Le-Bail, A. (2013). Effect of static  
712 electric field on ice crystal size reduction during freezing of pork meat. *Innovative Food*  
713 *Science & Emerging Technologies*, 20, 115–120.
- 714 Xanthakis, E., Le-Bail, A., & Ramaswamy, H. (2014). Development of an innovative  
715 microwave assisted food freezing process. *Innovative Food Science & Emerging*  
716 *Technologies*, 26, 176–181.
- 717 Xie, J., & Zhao, Y. (2003). Improvement of physicochemical and nutritional qualities of  
718 frozen Marionberry by vacuum impregnation pretreatment with cryoprotectants and

719 minerals. *Journal of Horticultural Science and Biotechnology*, 78(2), 248–253.

720 Zaritzky, N. E. (2000). Factors affecting the stability of frozen foods. In C. J. Kennedy (Ed.),  
721 *Managing frozen foods* (pp. 111–135). Cambridge: Woodhead Publishing Limited.

722 Zhao, Y., & Takhar, P. S. (2017). Micro X-ray computed tomography and image analysis of  
723 frozen potatoes subjected to freeze-thaw cycles. *LWT - Food Science and Technology*,  
724 79, 278–286.

725

726

727

728

729

730

731

732

733

734 **Captions for the Figures**

735 Figure 1: (a) Representative freezing curves obtained during control and MAF of apple. “AT”  
736 attached in the legend for each freezing condition relates to the ambient temperature  
737 maintained during the freezing processes. (b), (c), (d) and (e) Zoomed areas of time-  
738 temperature curves for the different freezing conditions.

739 Figure 2: (a) and (b) Frequency curves and cumulative pore size distributions of apple  
740 samples treated under various conditions. Control = no microwaves exposure, CMAF =  
741 constant microwave condition, and PMAF (includes both P1MAF and P2MAF) = Pulsed  
742 microwave conditions.

743 Figure 3: (a) Environmental SEM image of fresh apple; cryo-SEM images of apple under (b)  
744 control freezing condition, (c) CMAF condition, (d) P1MAF condition and (e) P2MAF  
745 condition. Abbreviations used in the above picture: A = air space, W = cell wall and  
746 membrane structure, IC = ice crystals. (f) and (g) Texture (firmness) and drip loss of apples  
747 after freezing under different freezing conditions. Values with different superscripts within  
748 the same graph differ significantly ( $p < 0.05$ ).

749 Figure 4: (a) Representative freezing curves obtained during control and MAF of potato. (b)  
750 Frequency curve and (c) cumulative pore size distribution of potatoes after freezing under  
751 control and MAF conditions. X-axis has a logarithmic scale.

752 Figure 5: Texture parameters (a) Hardness and (b) Young’s modulus of fresh, blanched and  
753 frozen-thawed potatoes. (c) Drip loss (%) from potato samples after freezing under control  
754 and MAF conditions. (d) Colour attributes of potatoes at different processing stages. Values  
755 with different superscripts within the same graph differ significantly ( $p < 0.05$ ).

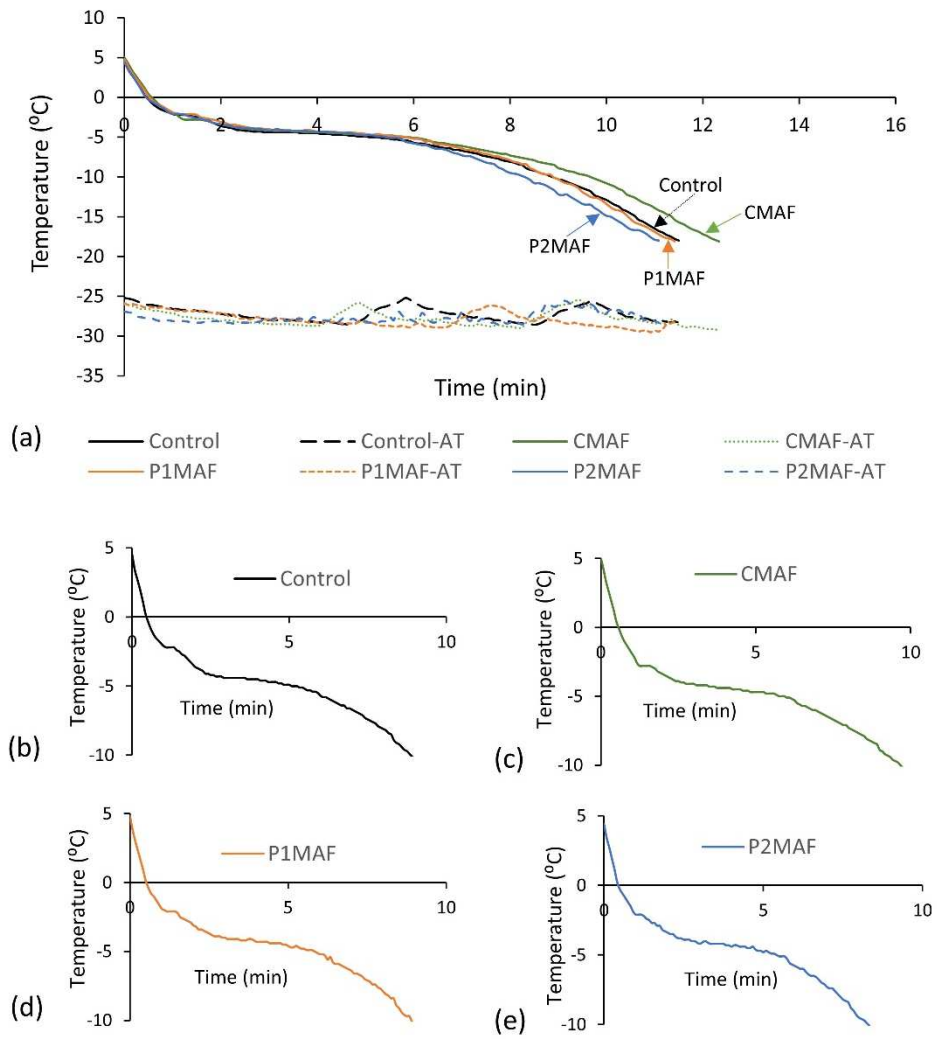
756

757 **Captions for tables**

758 Table 1. Freezing parameters and distribution characteristics of pores obtained during MAF of  
759 apple and potato samples. Values with different superscripts within the same column differ  
760 significantly ( $p < 0.05$ ).

761

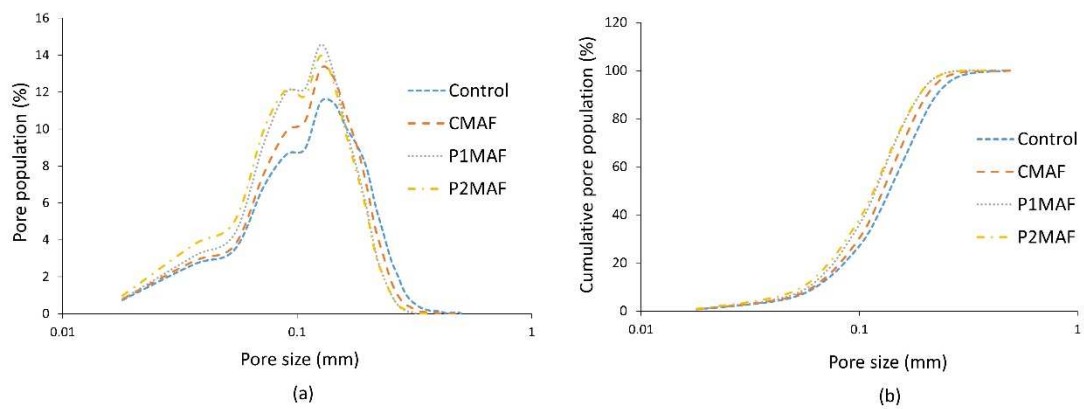
762 Figure 1.



763  
764  
765  
766  
767  
768  
769  
770  
771  
772

773 Figure 2.

774



775

776

777

778

779

780

781

782

783

784

785

786

787

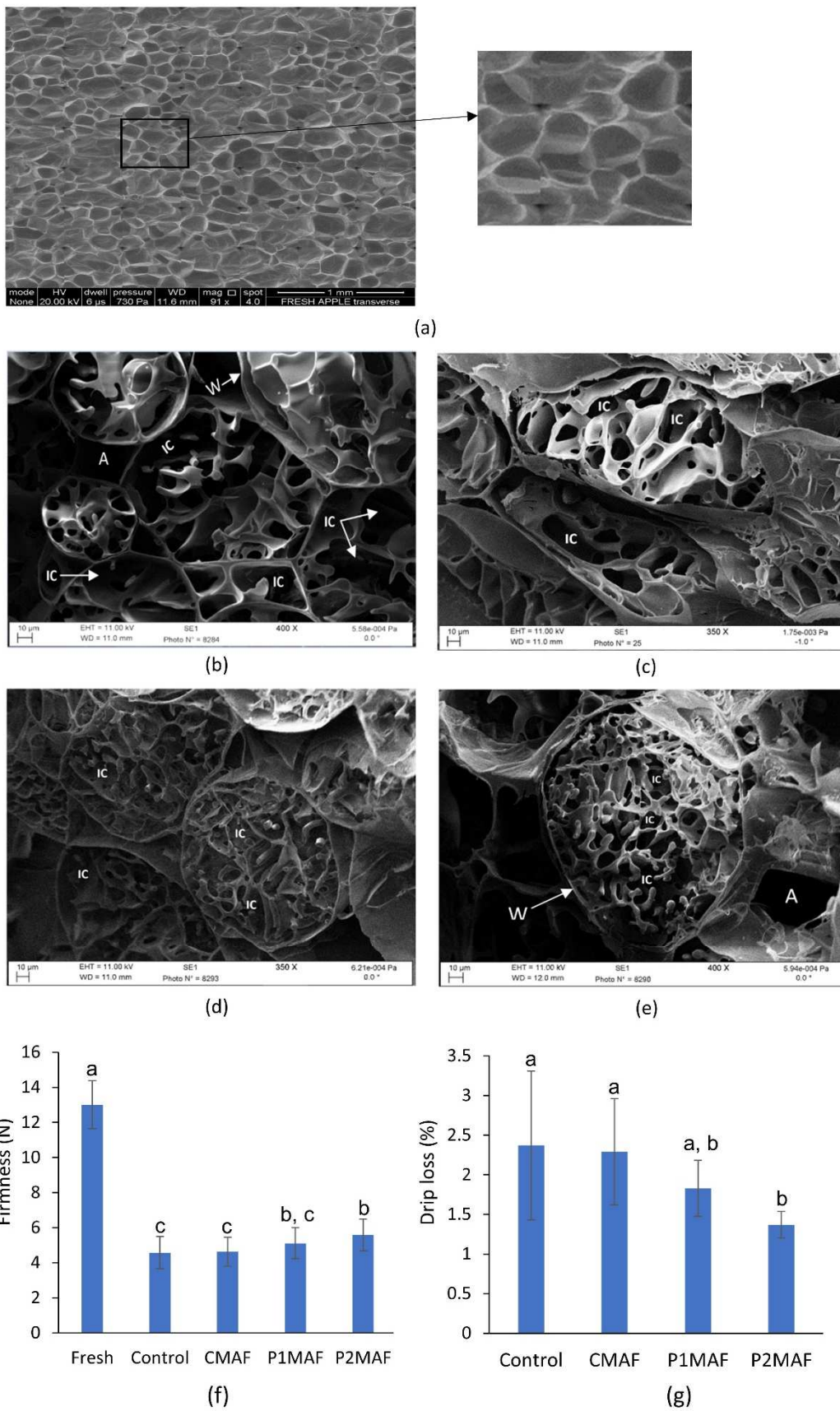
788

789

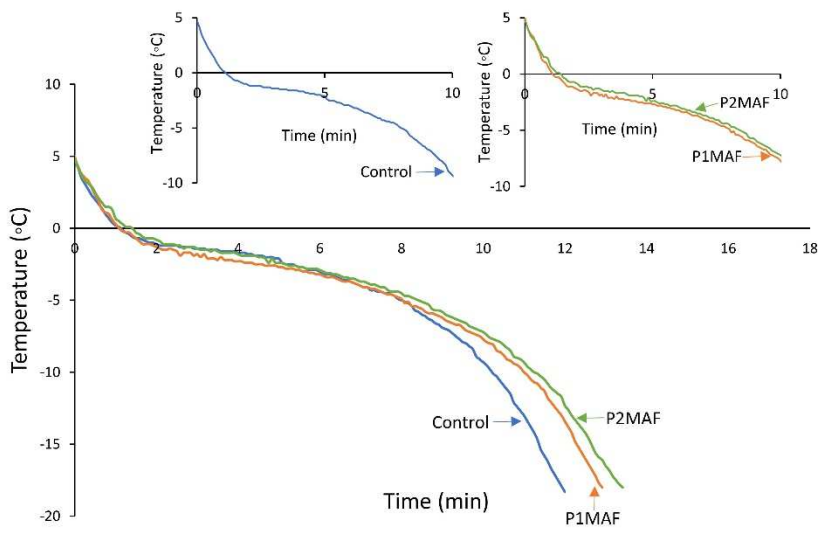
790

791

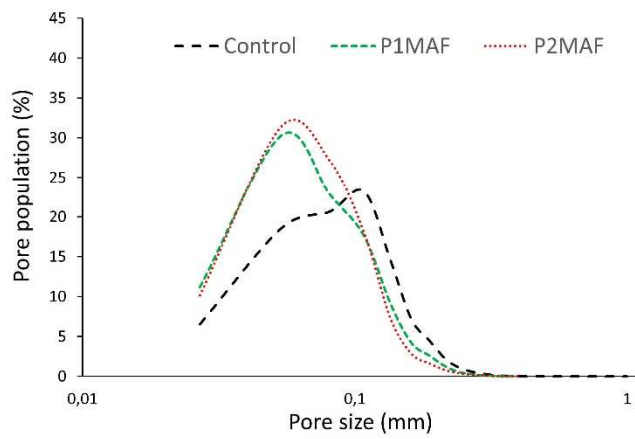
792



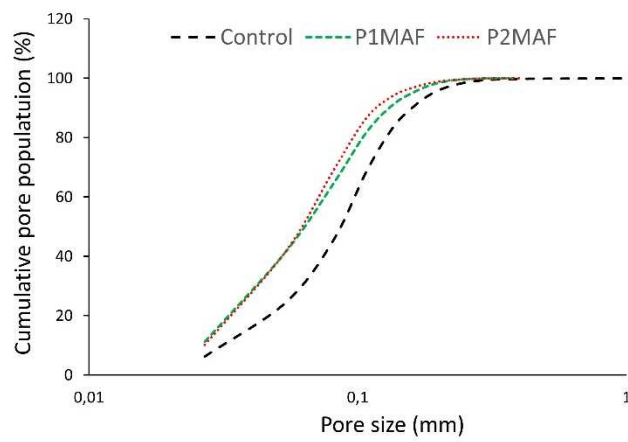
796 Figure 4



(a)



(b)



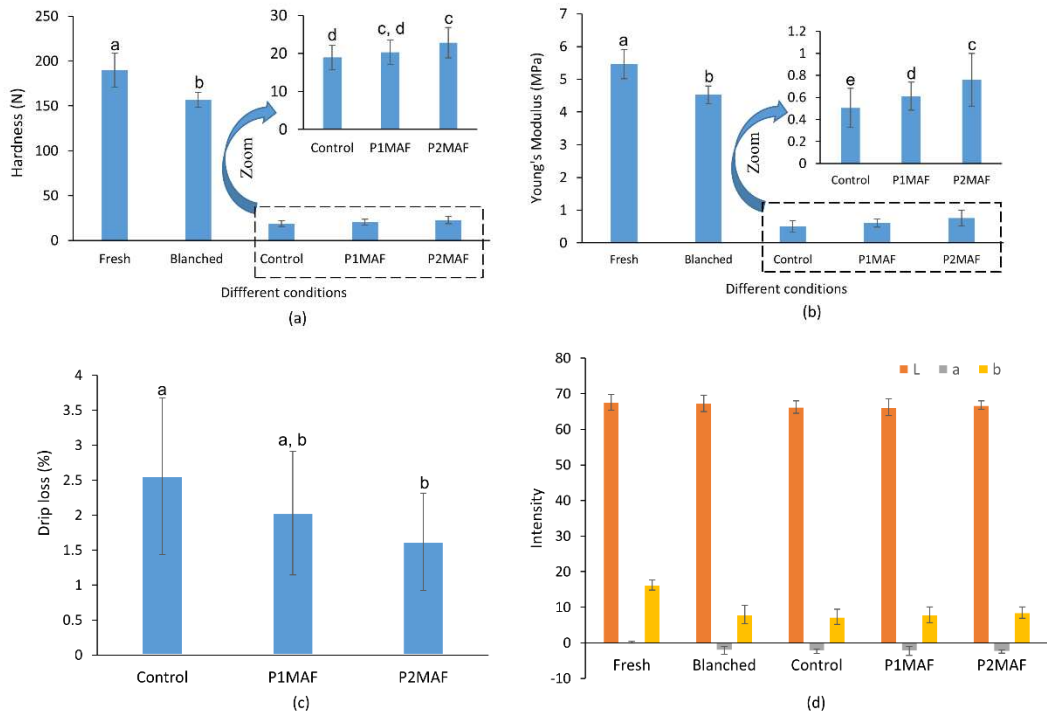
(c)

797

798

799 Figure 5.

800



801

802 Table 1.

803

804

Product	Freezing condition	Characteristic freezing time (min)	Overall freezing time (min)	Overall freezing rate (°C/min)	Mean pore size (µm)	D-Values		
						D10 (µm)	D50 (µm)	D90 (µm)
Apple	Control	6.58 ± 0.50 <sup>a</sup>	12.28 ± 0.79 <sup>a</sup>	1.88 ± 0.08 <sup>a</sup>	151.76 ± 7.45 <sup>a</sup>	62.53 ± 3.27 <sup>a</sup>	137.59 ± 5.86 <sup>a</sup>	227.21 ± 13.85 <sup>a</sup>
	CMAF	7.14 ± 0.55 <sup>a</sup>	12.36 ± 1.21 <sup>a</sup>	1.85 ± 0.17 <sup>a</sup>	140.46 ± 7.53 <sup>a, b</sup>	60.44 ± 1.70 <sup>a, b</sup>	128.77 ± 6.78 <sup>a, b</sup>	205.21 ± 16.52 <sup>a, b</sup>
	P1MAF	6.75 ± 1.54 <sup>a</sup>	11.92 ± 1.88 <sup>a</sup>	1.99 ± 0.30 <sup>a</sup>	129.64 ± 13.88 <sup>b</sup>	58.32 ± 4.40 <sup>a, b</sup>	119.41 ± 14.31 <sup>b</sup>	186.51 ± 21.08 <sup>b</sup>
	P2MAF	6.25 ± 0.52 <sup>a</sup>	11.89 ± 1.40 <sup>a</sup>	1.96 ± 0.20 <sup>a</sup>	127.63 ± 4.63 <sup>b</sup>	53.93 ± 4.16 <sup>b, c</sup>	116.32 ± 3.57 <sup>b</sup>	189.16 ± 7.17 <sup>b</sup>
Potato	Control	7.24 ± 0.40 <sup>a</sup>	11.71 ± 1.27 <sup>a</sup>	1.98 ± 0.20 <sup>a</sup>	105.52 ± 4.66 <sup>a</sup>	33.42 ± 4.94	85.59 ± 5.16 <sup>a</sup>	162.93 ± 20.54 <sup>a</sup>
	P1MAF	7.58 ± 1.04 <sup>a</sup>	12.47 ± 1.47 <sup>a</sup>	1.83 ± 0.18 <sup>a</sup>	85.86 ± 17.68 <sup>a, b</sup>	-	66.45 ± 19.29 <sup>a, b</sup>	127.92 ± 27.59 <sup>a, b</sup>
	P2MAF	7.69 ± 0.21 <sup>a</sup>	12.81 ± 0.55 <sup>a</sup>	1.79 ± 0.08 <sup>a</sup>	82.10 ± 6.31 <sup>b</sup>	-	59.95 ± 7.58 <sup>b</sup>	115.86 ± 9.98 <sup>b</sup>

805

806